Proceedings of the XIth International Congress and Exposition
June 2-5, 2008 Orlando, Florida USA
©2008 Society for Experimental Mechanics Inc.

Observation of Composite Materials Using Coupled Mechanical Testing and Computed Tomography

Vlastimil Kunc, Research Staff Member
Oak Ridge National Laboratory, Post Office Box 2008, Oak Ridge, TN 37831-6053,
kuncv@ornl.gov

Donald Erdman, Barbara Frame, Robert Norris,
Oak Ridge National Laboratory

Scott Case
Virginia Polytechnic Institute and State University

Abstract

A coupled load frame and x-ray micro-tomography unit was used to observe damage processes occurring within model composite specimens subjected to mechanical loading. These specimens consisted of two tows of glass fiber in the form of bound loops within an epoxy matrix of cylindrical form with 3-mm diameter cross-section. Computed tomography reconstruction was used to investigate internal structure of the specimens under load. This reconstruction revealed internal cracking and progressive failure in several experiments.

Introduction

The use of composites over the past six decades has been driven by high-end structural applications where design is governed by specific stiffness, strength or fatigue life considerations and where no single homogeneous material could be used [1]. To support these designs, investigations of damage processes in the composites were used primarily to establish failure criteria and in turn to design material with higher threshold for damage. Most studies in the field were oriented on design and analysis of composites under standard service conditions, therefore energy absorption of composite structures was not the primary concern. As composites are increasingly applied in automobiles and other structures where behavior during abnormal service events, such as crash, is of considerable importance, energy absorption is being investigated. Some composites have been found to possess good energy absorption properties; however, empirical investigations and phenomenological models for given

material combinations and fiber architectures appear to dominate this field. Designers wishing to tailor the internal structure of composite material reinforced with continuous fibers can use readily available tools and design guidelines to investigate numerous options prior to making an actual test article. These tools will likely give good predictions for stiffness analyses and, when used with a large amount of published experimental data, provide reasonable predictions for strength analyses. Multi-scale modeling tools [2,3] can be used to estimate energy absorption of composite structures, however confidence in predictive capabilities of these tools may suffer due to the inability to support assumptions about progressive damage on the microscopic scale by direct observation of multiple damage processes being active. When designing for maximum strength, it is usually preferable to delay initial damage in the material until high load is achieved in the structure and it is important to make sure that failure occurs in the fiber direction rather than relying on other, matrix property dominated, failure mode. Reducing the number of damage mechanisms being active in the material prior to failure and increasing threshold load for initial damage is the usual objective in design and analysis of composite structures. As long as multi-scale modeling tools capture the limited number of dominant failure modes, they are useful for strength driven design. In contrast, the objectives in designing composite structures for maximum energy absorption differ significantly. Energy absorbing structures are often used to protect passengers in a vehicle or electronics in an enclosure by reducing inertial forces during incidents and rough handling. This is best achieved by triggering initial damage early and dissipating energy through multiple damage modes. Instead of minimizing the number of damage modes and maximizing the initial damage threshold as in strength driven design, maximum number of damage modes and early onset of damage is usually desirable in energy absorbing structures. A thorough understanding of possible damage modes is therefore necessary in order to develop reliable predictive tools for energy absorption modeling. This understanding is dependent on techniques used to observe the damage modes. Data collected on the surface of test articles via strain gages, extensometers or optical methods [4] along with visual observation of samples and microscopy of failure surface [5] are traditionally the primary tools for evaluation of processes being active within material. Acoustic emission can be used to monitor the nature and location of damage if the process is audible [6]. Micro-cracking is also often observed using x-ray imaging of a penetrating liquid deposited in the cracks [7]. The techniques listed above are well established and their use is widespread; however they do not allow direct observation of specimens subjected to load—one is left to infer and model the events that took place in the composite. To address this gap, a tensile testing machine capable of operating inside a 3-D x-ray tomography machine is being developed at the Oak Ridge National Laboratory (ORNL). This new and unique capability allows examination or processes occurring in materials and viewing of specimens under load in various stages of damage in three dimensions.

Specimen preparation

Substantial effort was devoted to developing a procedure for sample manufacturing. The goal in specimen preparation was to obtain repeatable samples with controlled fiber architecture, material properties, interface properties and with geometry that would lead to failure in the area of interest. Three epoxy resin systems were evaluated in an effort to obtain desired "ductile" and "brittle" matrix behavior. While it was possible to achieve very brittle behavior in one system, it was not possible to manufacture specimens with this system without incurring

damage prior to mounting of the sample in the testing machine. It was also not possible to obtain necking prior to failure with the epoxy systems under consideration. Preparation procedures were identical for all three epoxy systems, however handling and curing times may vary. The procedure is discussed in detail below for Epon 862 resin and 30 phr Ancamine 2167 hardener. Small tow E-glass [8] was used to make the desired fiber form. The fiber form had a shape of two interconnected loops. The loops were continuous (Figure 1) or interrupted at a pre-determined location (Figure 2).

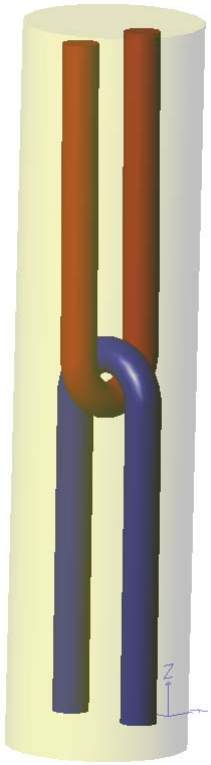

Figure 1. Schematic of fiber form within a specimen with continuous fiber tow loops.

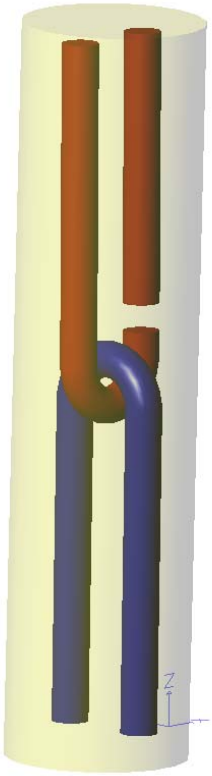

Figure 2. Schematic of fiber form within a specimen with interrupted fiber tow loops.

A cylindrical specimen rod was formed around the fiber form and grip pieces were bonded to the end of the specimen rod using a fixture. Several design iterations of grip pieces were conceived and experimented with to reduce excessive specimen relaxation under load, specimen rod pull-out and fracture near the grip piece (Figure 3).

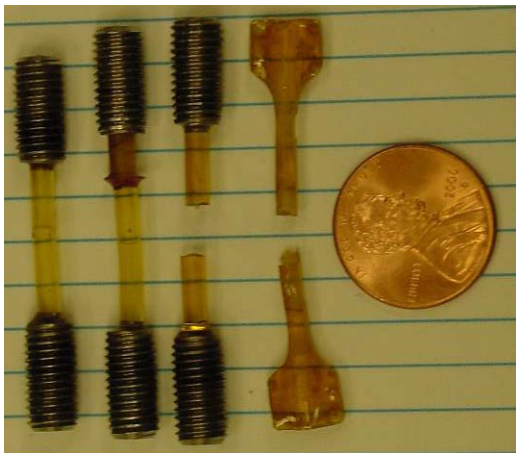

Figure 3. Untested specimen, specimen with pulled out grip piece, specimen with gage length grip failure and initial specimen design.

This effort was only partially successful since grip failures were not eliminated for any of the design iterations. The final design of the grip piece is illustrated in Figure 4. A stainless steel threaded rod (1/4-28) 0.25 inches long was drilled with a tapered drill bit and the wide part of the hole was subsequently plugged by welding it.

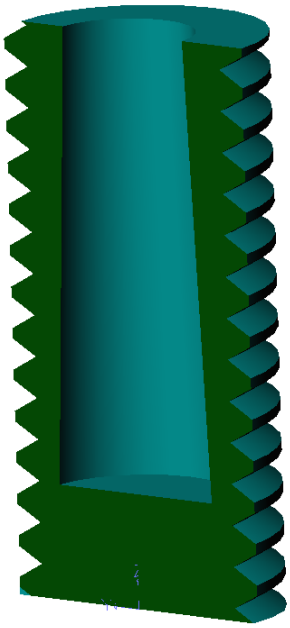

Figure 4. Cross-section of final design of the grip piece.

The following steps were followed to make "loop samples":

1. Cut two 18 inch long strands of glass tow and create a loop. Bond the ends of the strands with cyano-acrylate adhesive for easy handling. If reduced fiber matrix adhesion is desired, coat the tow in mold release and allow to dry.
2. Cover a flat surface with mold release film and affix stripes of high temperature tape 5 inches apart.

3. Mix epoxy, deposit loops in the resin and heat up to 60°C, until most bubbles disappear. De-gas resin with the loops.
4. Extract loops impregnated with resin and remove excess adhesive.
5. Affix stretched out loops with high temperature tape and cure the epoxy to obtain fiber form (Figure 5).

Figure 5. Fiber form with cured epoxy maintaining the shape.

6. Cut the fiber form into an appropriate length and cut the strands if desired. Insert the fiber form into a Teflon tube and seal the bottom with clay (Figure 6).

Figure 6. Fiber form (right) was inserted in Teflon tube and bottom sealed with clay (middle) to produce a specimen (left).

7. Mix epoxy, heat up to 60°C until most bubbles disappear and de-gas. Fill syringe with the epoxy and attach hypodermic needle
8. Pierce the clay at the bottom of the tube and slowly inject the epoxy. Withdraw the needle and seal the opening thoroughly with clay to prevent leaks. Insert the Teflon tube in a copper tube in vertical position to make the Teflon tube straight and to prevent leaks. Let the epoxy gel and then cure.
9. Withdraw the Teflon tube from the copper tube. Pull out the specimen rod if possible. It may be necessary to cut away the Teflon tube. Cut the specimen rod to appropriate length.

10. Clean the grip pieces thoroughly, wrap the threads in Teflon tape and insert them in the alignment fixture. Mix epoxy, heat up to 60°C along with an empty syringe, grip pieces and alignment fixture. Fill the syringe and deposit a few drops in a warm grip piece. Rotate the specimen rod while slowly inserting it in the grip piece. Place a loose grip piece at the top of the rod. Cure the epoxy. Remove specimens from the alignment fixture and repeat step 8 to bond grip piece to the other end of the grip piece.

Experimental Setup

The test setup consists of a micro-tomography unit produced by X-radia Inc. and a custom screw driven testing machine operating within the tomography unit (Figure 7) with accompanying data acquisition and control equipment.

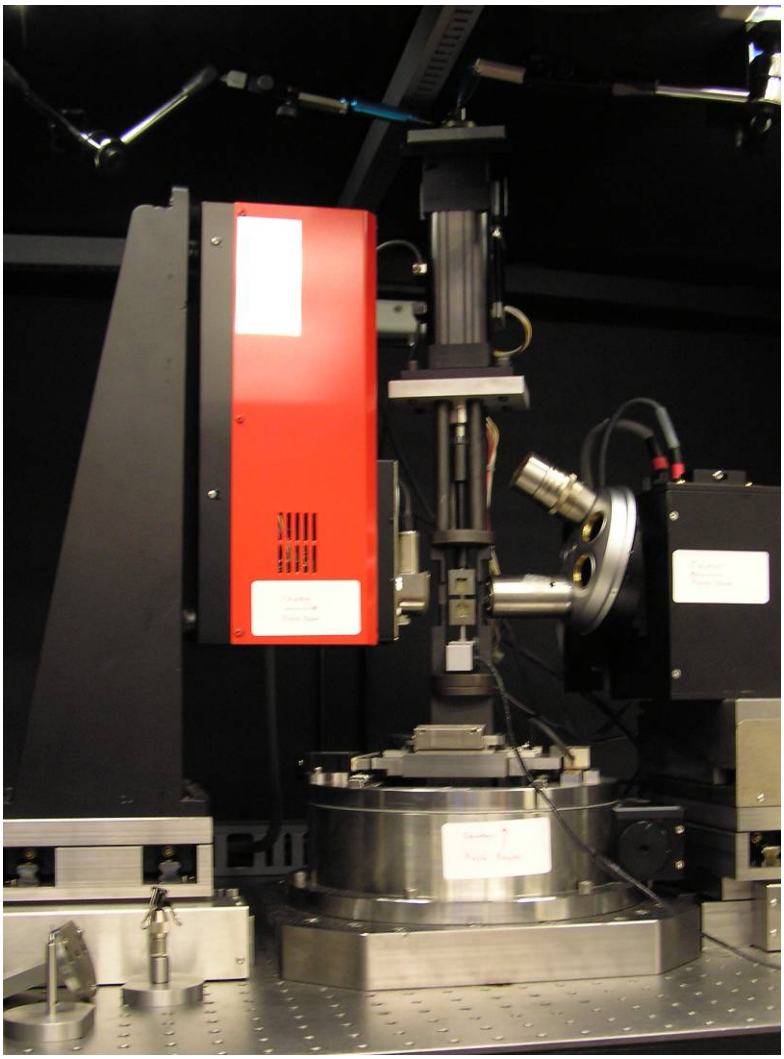

Figure 7. Testing machine within x-ray micro-tomography unit.

The primary components of the micro-tomography unit are the source, detector and x-y-z-rotate stage [9]. The source and the detector are also on stages to allow proper alignment. A 40 - 150 keV x-ray source allows through

penetration imaging. The detector contains a 2048x2048 pixel, 16 bit CCD camera and two objectives (3.8x and 19.8x). The 3.8x objective was used for the study presented below.

The ORNL-designed test system is based on a screw driven testing machine with 1.33 kN (300 lb) capacity that can test specimens of up to 3 mm (0.118 in.) cross-section. An Interface load cell [10] is used to measure load and displacement is measured by the actuator encoder. Custom software was written in LabView [11] for data acquisition and control of the system.

The tomography unit and the testing machine are connected to two separate computers and synchronization is performed manually. Details regarding the experimental setup are expected to be published later this year [12].

Testing Procedure

Alignment of the system is performed once before a set of tests is performed. The testing machine is attached to a fixed bearing at the top and to the x-y-z-rotate stage at the bottom. The objective of alignment is to assure that the axis of the stage is aligned with the axis of the bearing. This will result in minimal forces on the stage positioning motors and minimal wobble of the sample during rotation of the instrument. The precision of alignment is judged from the movement of a small tungsten carbide ball deposited in an epoxy specimen rod. The specimen rod was made using the technique discussed above with the fiber form not being present. The ball was deposited into a small hole that was drilled in the specimen rod and the hole subsequently sealed with an adhesive. During alignment, the specimen rod can be treated as transparent and only the movement of the ball was monitored. Figure 8 and Figure 9 show vertical and horizontal wobble of the ball through 150 degrees of rotation. The amount of wobble is less than for samples mounted on the stage without the testing machine present. This is likely due to the additional constraint being present at the top of the testing machine.

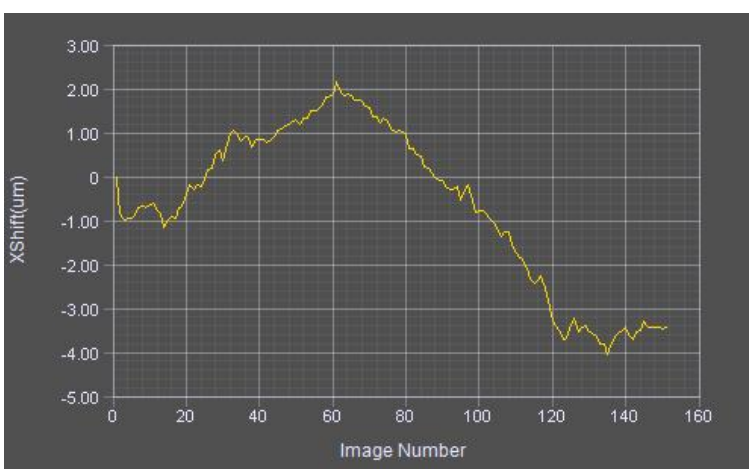

Figure 8. Horizontal wobble of alignment ball through 150 degrees of rotation.

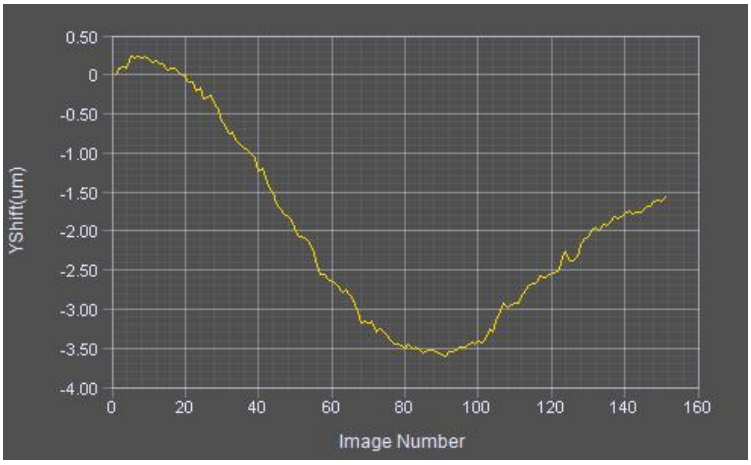

Figure 9. Vertical wobble of alignment ball through 150 degrees of rotation.

Once the alignment was completed, a set of tests was performed and the known wobble could be corrected using software.

After the specimen was mounted in the testing machine, it was loaded to a low load level to eliminate slack in the system. The sample was then loaded in displacement control with a stroke rate of 0.005 in./s. Loading was performed in steps with pauses in which displacement was held constant at initial pre-determined load levels. These pauses allowed imaging and examination of the sample. Although the sample relaxed and the load decreased during the pause, two dimensional x-rays show individual fibers clearly and tomography reconstruction also provides valuable insight into the processes in the material. The time to complete each individual x-ray, excluding manual operation of the computer, is 9.5 seconds (5 second exposure with 4.5 seconds of data transfer overhead). With additional overhead for rotating the stage, the total time to complete tomography imaging with 1000 exposures is three hours. Tomography was performed before loading and at times when interesting behavior was observed during loading and after gage-length failure.

Results and Observations

As indicated in the above discussion, grip failures were not eliminated; therefore observation of processes occurring in the material leading to failure was not possible for some of the specimens. There were several preliminary tests performed, primarily to establish the testing procedure and to experiment with various epoxy formulations and gripping techniques. Three replicates of three types of samples were tested. The first type contained a fiber form with a continuous loop of un-modified tow. All of these specimens failed at the grip and no significant processes were observed prior to failure. The second type of specimens contained fiber form with a continuous loop of tow coated in mold release. Two of the three specimens failed within the gage length and some observations are discussed below. The third set of specimens contained fiber form with an un-modified, but interrupted tow. One tow was cut approximately 1 mm from the loop end (Figure 10).

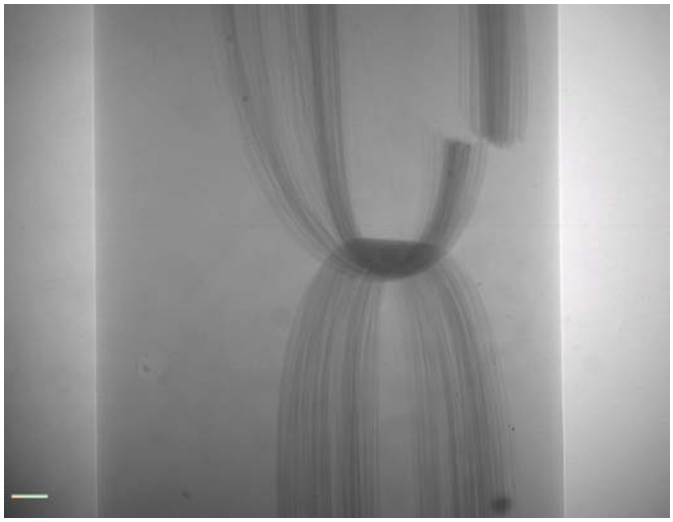

Figure 10. X-ray image of fiber form with interrupted tow (CutLoop1).

It was speculated that the fiber ends in close proximity of the loop would act as stress concentrators, which would initiate or alter failure mechanism of the sample. However, all specimens tested failed at the grip indicating the need to further refine the testing technique. Table 1 represents the final set of tests performed with the knowledge gained during the experimentation.

Table 1. Test Matrix

Specimen Name	Specimen Type	Test Notes
FullLoop1	Full loop, no mold release	Grip failure at 60.2 lb.
FullLoop2	Full loop, no mold release	Grip failure at 59.6 lb.
FullLoop3	Full loop, no mold release	Grip failure at 68.9 lb.
FullLoopMoldRel1	Full loop, mold release on tows	Observed white region at 30 lb. Gage length failure at 54.3 lb. Top loop failed completely.
FullLoopMoldRel2	Full loop, mold release on tows	Did not observe damage before failure. Gage length failure at 48.1 lb.
FullLoopMoldRel3	Full loop, mold release on tows	Observed crack at 24 lb. Data acquisition malfunction.
CutLoop1	Loop cut 1 mm from the loop end, no mold release	Grip failure at 60.2 lb.
CutLoop2	Loop cut 1 mm from the loop end, no mold release	Grip failure at 78.6 lb. Possible data acquisition malfunction during final loading.
CutLoop3	Loop cut 1 mm from the loop end, no mold release	Grip failure at 51.2 lb

Observations of FullLoopMoldRel1 (Figure 11) are presented below. Similar observations were made during testing of FullLoopMoldRel2 and experimental samples with fiber tow sizing not optimized for epoxy matrices.

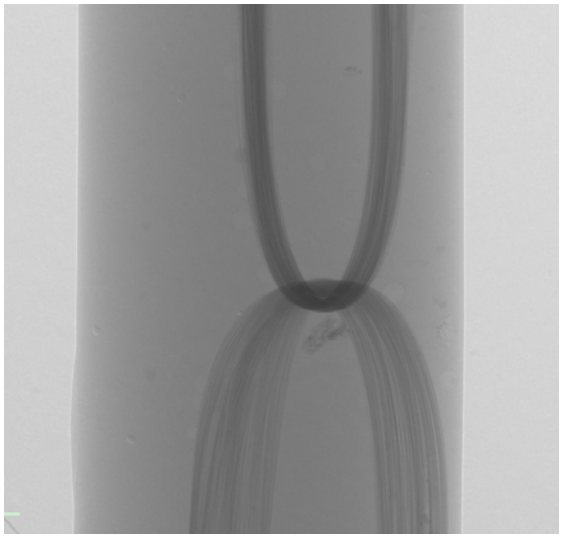

Figure 11. X-ray of FullLoopMoldRel1 specimen showing observable gage length.

Figure 12 shows the load-displacement curve for FullLoopMoldRel1 specimen. Loading of this sample was performed in 3 lb increments, which can be detected in the load-displacement curve. A large drop in load can be observed at 30 lb and another drop at 42 lb. These correspond to relaxation of the sample during tomography imaging at 30 lb and extended examination at 42 lb.

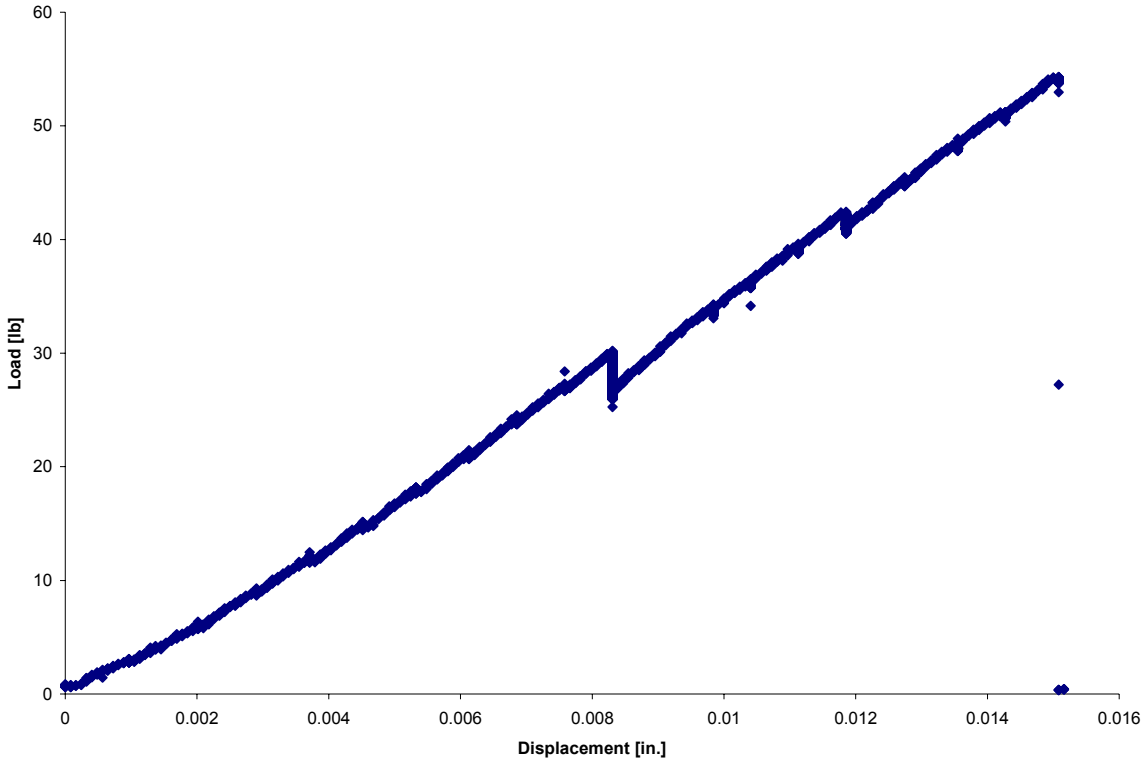

Figure 12. Load-displacement curve for the entire test of FullLoopMoldRel1.

A load-time curve shown in Figure 13 indicates relaxation of the specimen during each pause in loading leading up to the tomography imaging, which was started with the specimen carrying approximately 29 lb. This tomography was performed because a new crack was observed in the sample. Figure 14 shows relaxation of the specimen during tomography imaging.

After the tomography imaging was completed, the specimen was again loaded in steps with an extended observation performed at 42 lb load level (Figure 15). Maximum achieved load was 54.3 lb.

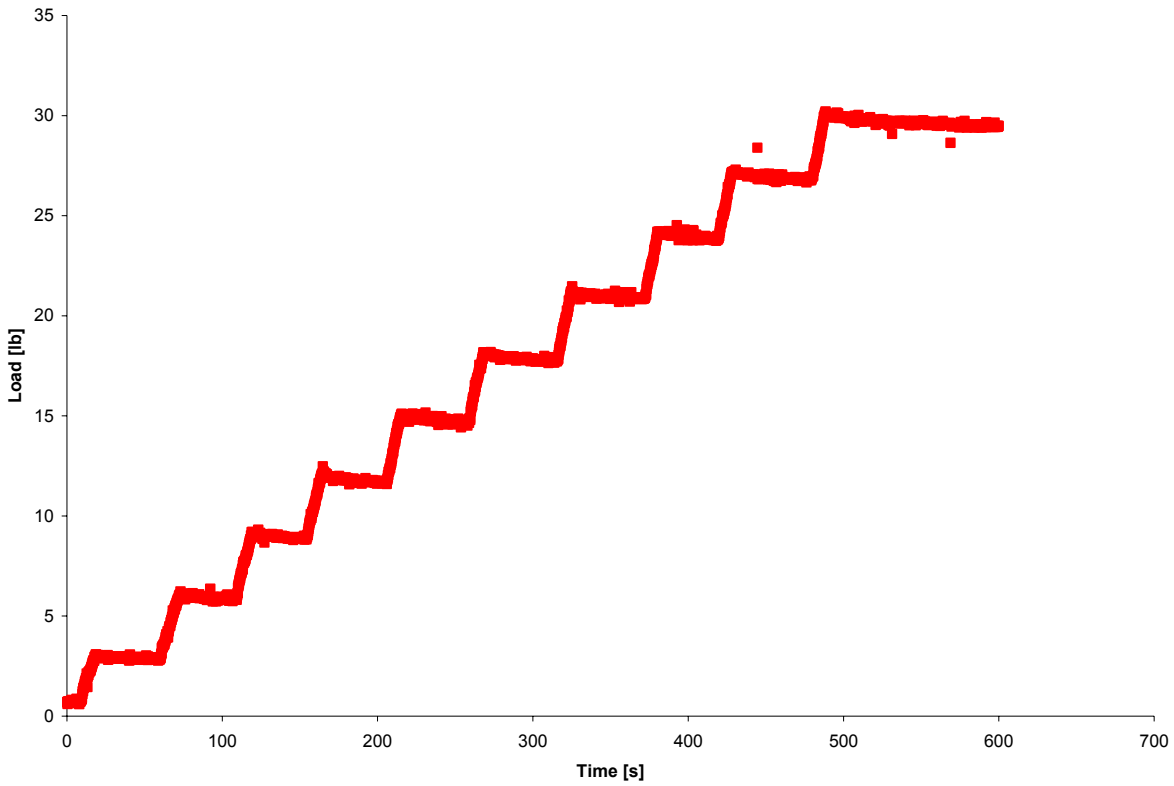

Figure 13. Initial ten minutes of loading leading up to tomography imaging at approximately 29 lb.

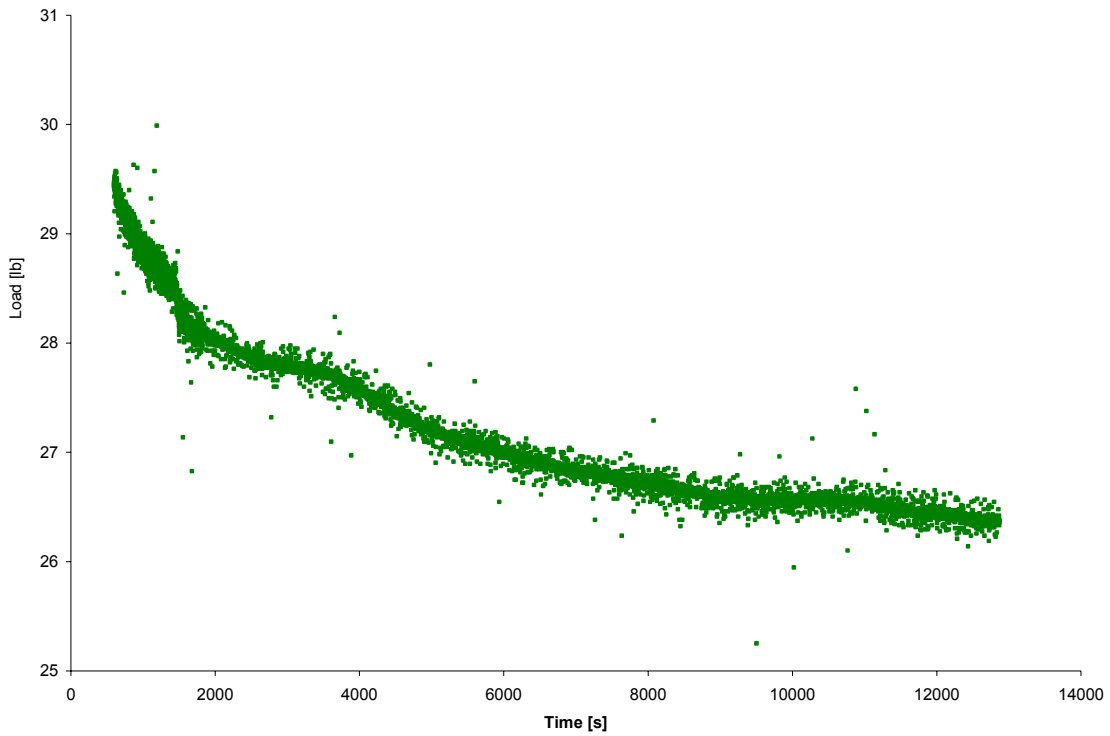

Figure 14. Relaxation of specimen during tomography imaging.

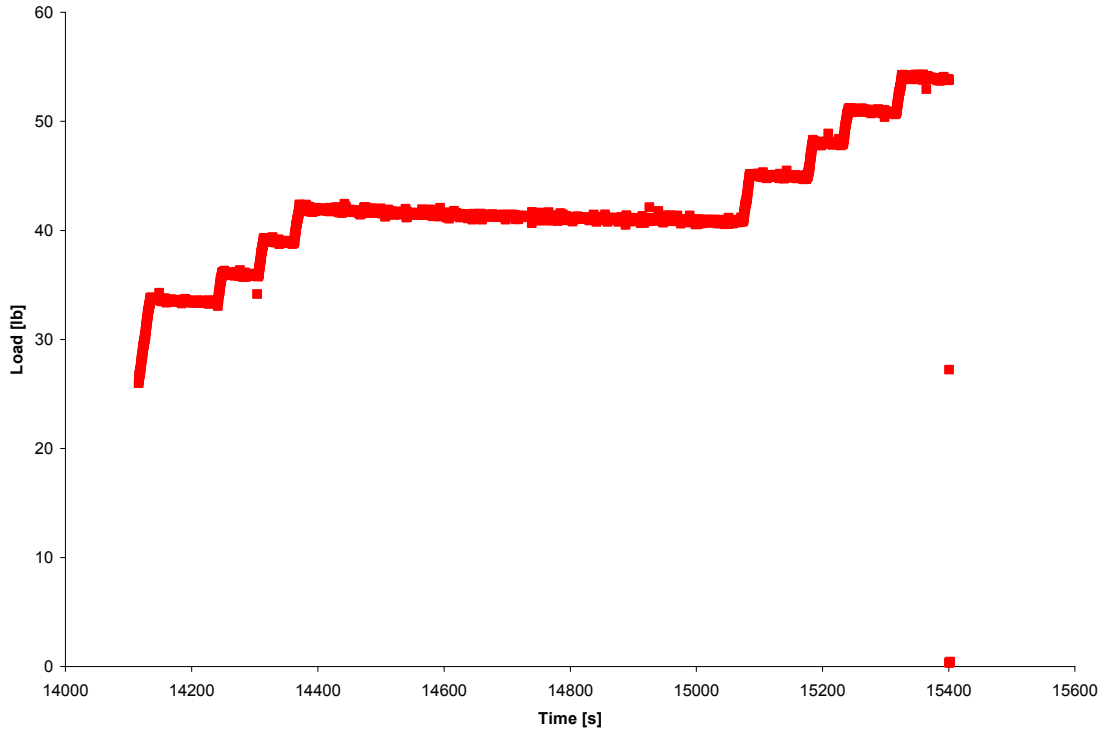

Figure 15. Loading after tomography taken at 29 lb with extended observation at 42 lb and failure.

Figure 16 and Figure 17 show details of x-ray images at no load and at approximately 29 lb. The specimen subjected to load exhibits a crack opening that was not present during the initial imaging before loading. This fact triggered the decision to perform tomography imaging. The quality of reconstruction suffers when the specimen relaxes during imaging as can be seen from Figure 18 and Figure 19, however single filaments can still be observed.

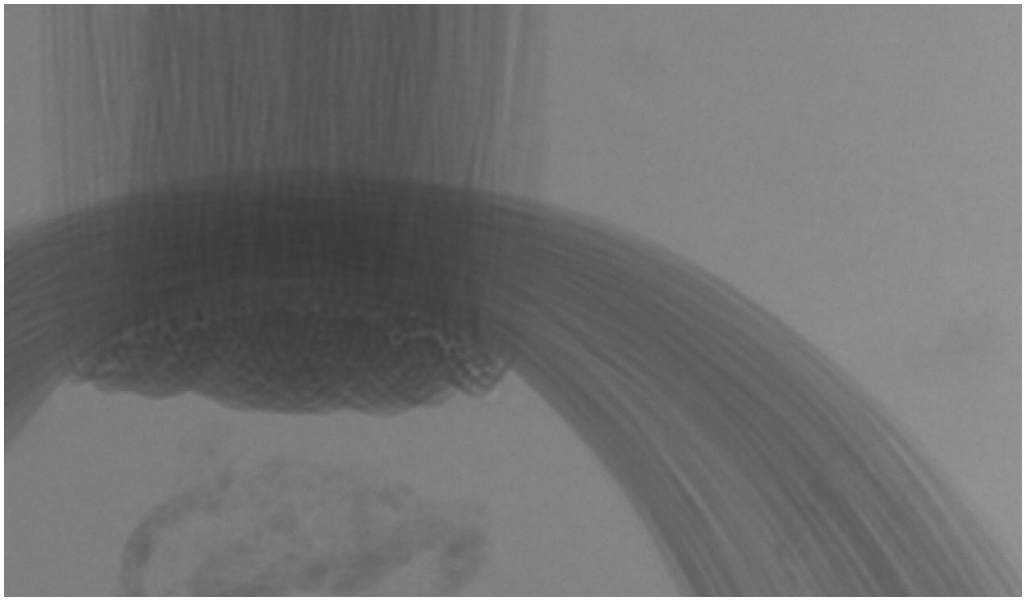

Figure 16. Detail of x-ray image of sample before loading.

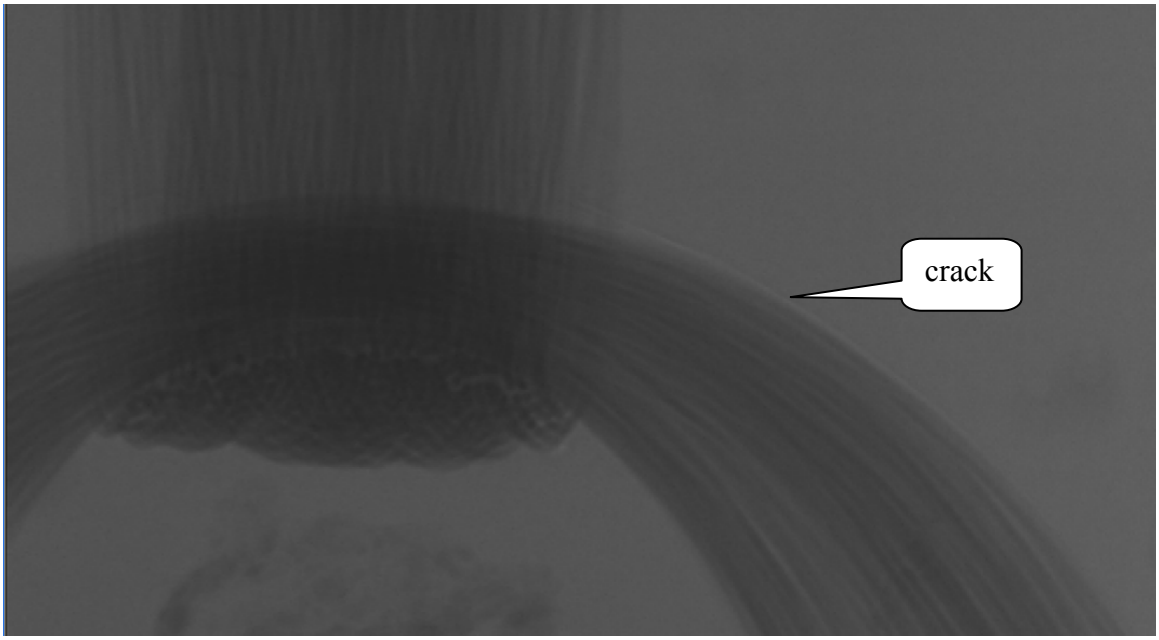

Figure 17. Detail of x-ray image of sample carrying approximately 29 lb of load.

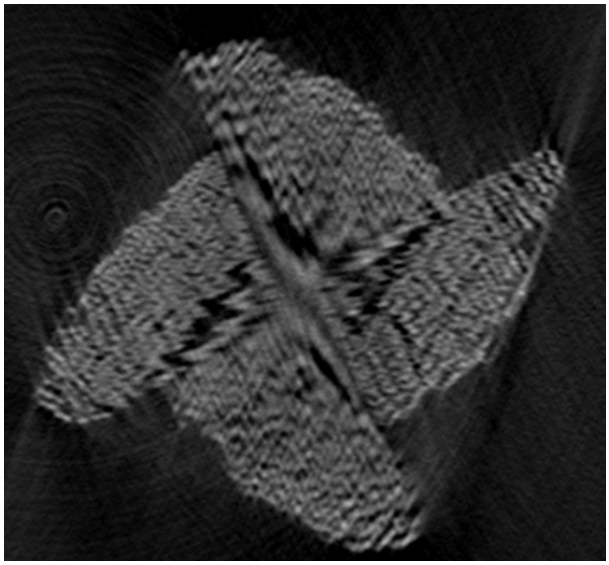

Figure 18. Detail of tomography reconstruction at no load - horizontal slice of the loop.

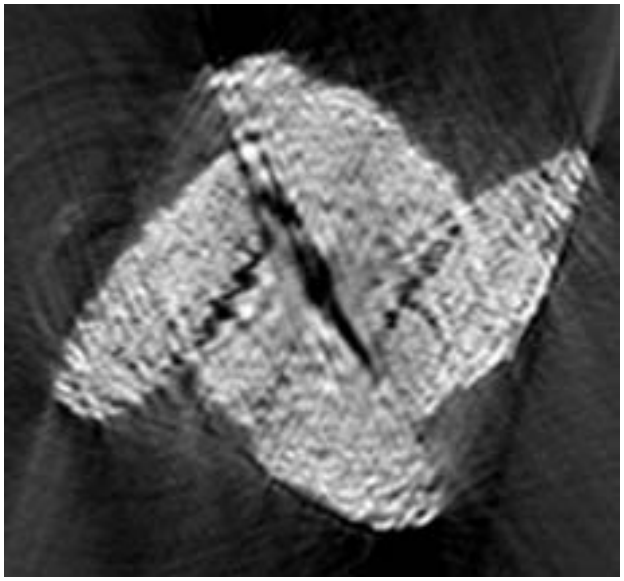

Figure 19. Detail of tomography reconstruction of sample subjected to load - horizontal slice of the loop.

Figure 20 and Figure 21 show slices of tomography reconstructions with no load and with specimen under load respectively. These slices are oriented at approximately 90 degrees to the imaging direction of Figure 16 and Figure 17. The crack can be tracked by inspecting multiple slices of the reconstruction.

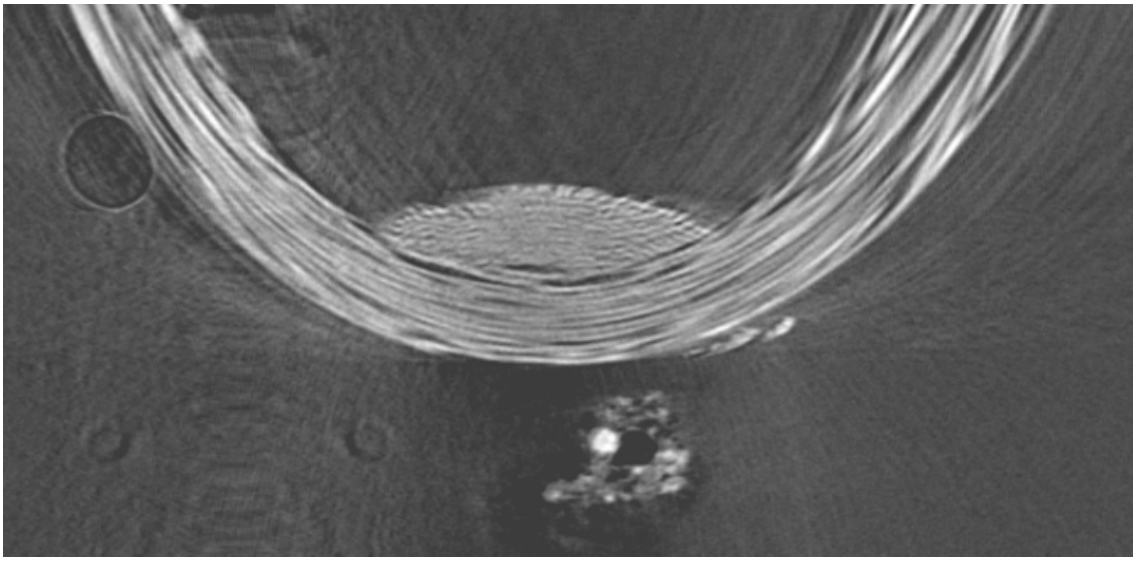

Figure 20. Vertical slice of tomography reconstruction at no load.

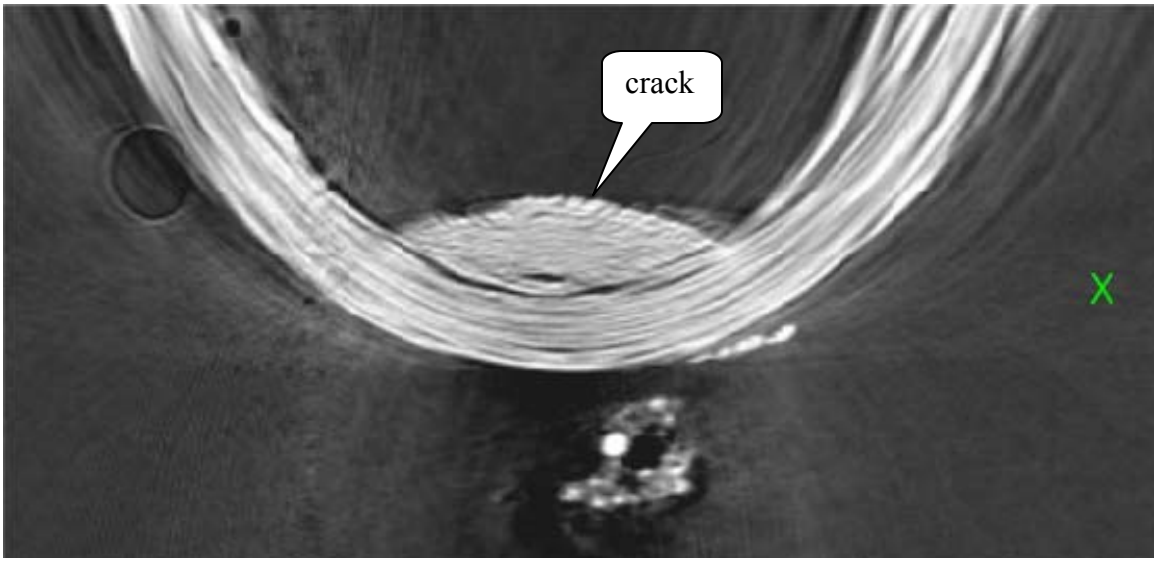

Figure 21. Vertical slice of tomography reconstruction of specimen under load showing crack within the specimen not observable prior to loading.

Another method of visualizing the internal structure of the sample is to render the tomography reconstruction and highlight certain features. Figure 22, Figure 23, and Figure 24 show renderings of tomography reconstruction of the fiber form at no load, at approximately 29 lb and after failure. This rendering can be achieved by making all parts of the reconstruction invisible with the exception of locations with the most x-ray absorption.

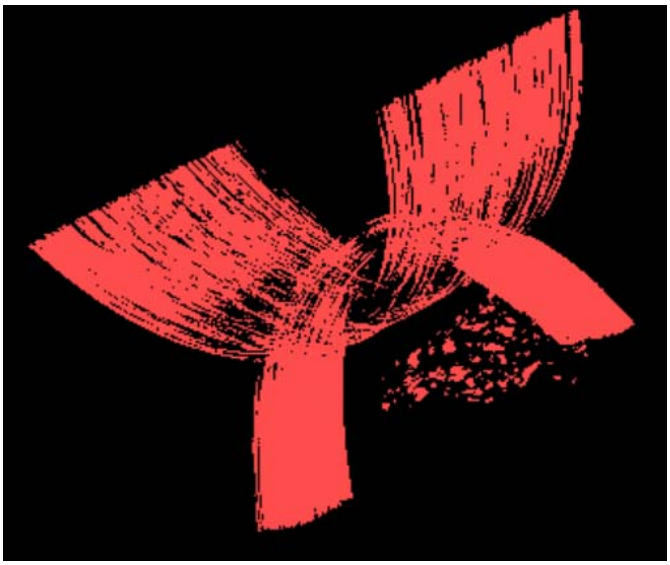

Figure 22. Rendering of fiber form at no load.

Figure 23. Rendering of fiber form inside specimen subjected to load.

Figure 24. Rendering of fiber form after failure.

Figure 25 and Figure 26 show renderings of locations with maximum and minimum x-ray transparency. As in previous images, the fiber form is rendered in red, while the areas of maximum x-ray transparency are displayed as blue and green. Air surrounding the cylindrical specimen is clearly visible along with two voids near the specimen rod surface. Closer examination reveals smaller voids and cracks in the vicinity of the fiber form, however these are obscured by reconstruction artifacts. Further work on data processing and visualization is necessary in order to clearly separate physical features and reconstruction artifacts.

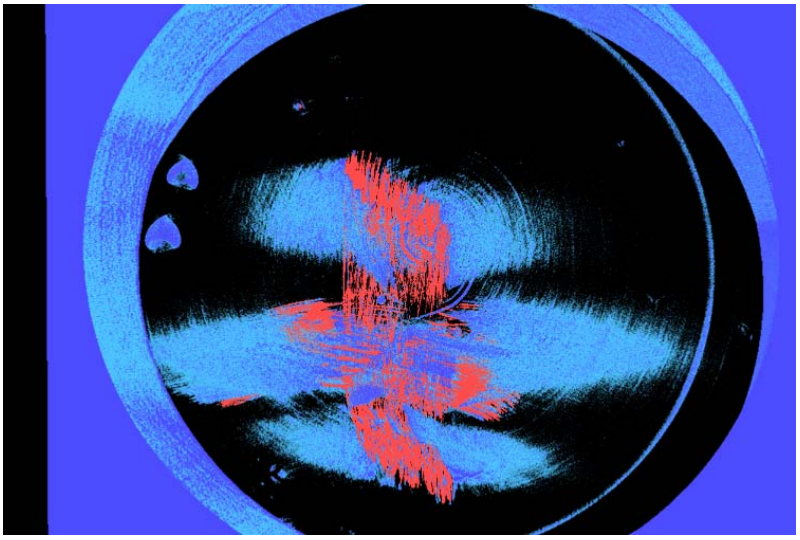

Figure 25. Rendering of fiber form and voids of specimen at no load, view from the top.

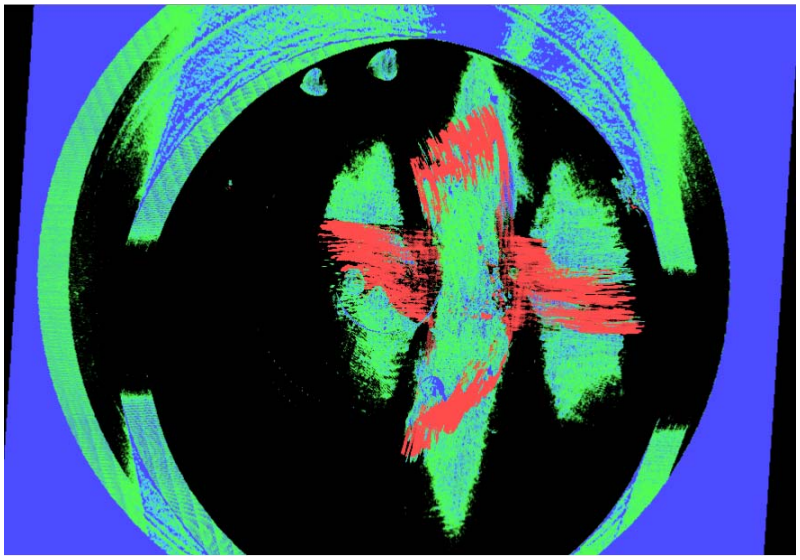

Figure 26. Rendering of fiber form and voids of specimen subjected to load, view from the top.

Visualization of areas with maximum x-ray transparency of the failed specimen does not yield useful results. Instead, locations with x-ray absorption close to that of the matrix material are visualized in green, while x-ray transparent locations are not viewed. It is possible to visualize crack surfaces of the failed sample using this rendering; however, examination of reconstruction slices provides a more accurate picture of the actual material-air boundary.

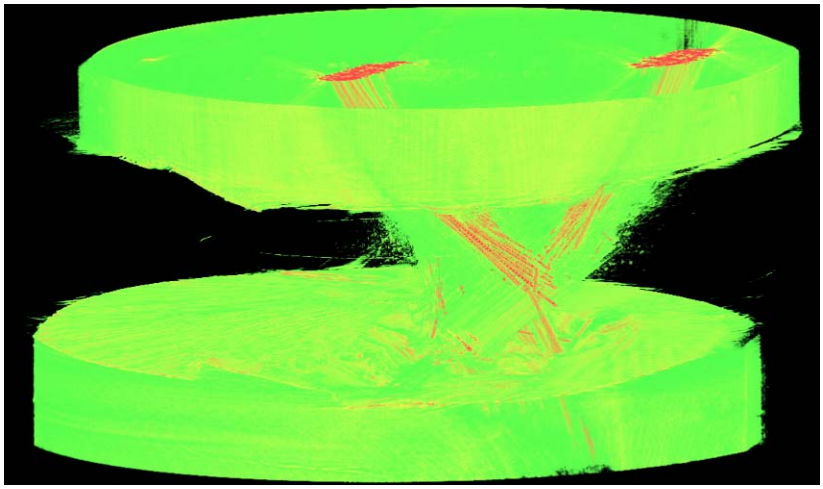

Figure 27. Rendering of fiber form and matrix after failure.

Figure 28 shows a selection of reconstruction slices of the failed specimen. The fiber form is clearly visible in light color, while crack surfaces are between the black regions (air) and gray regions (matrix). Examination of reconstruction slices reveals not only the shape of the primary crack surface, but also numerous internal cracks and cracks nearly perpendicular to the primary crack.

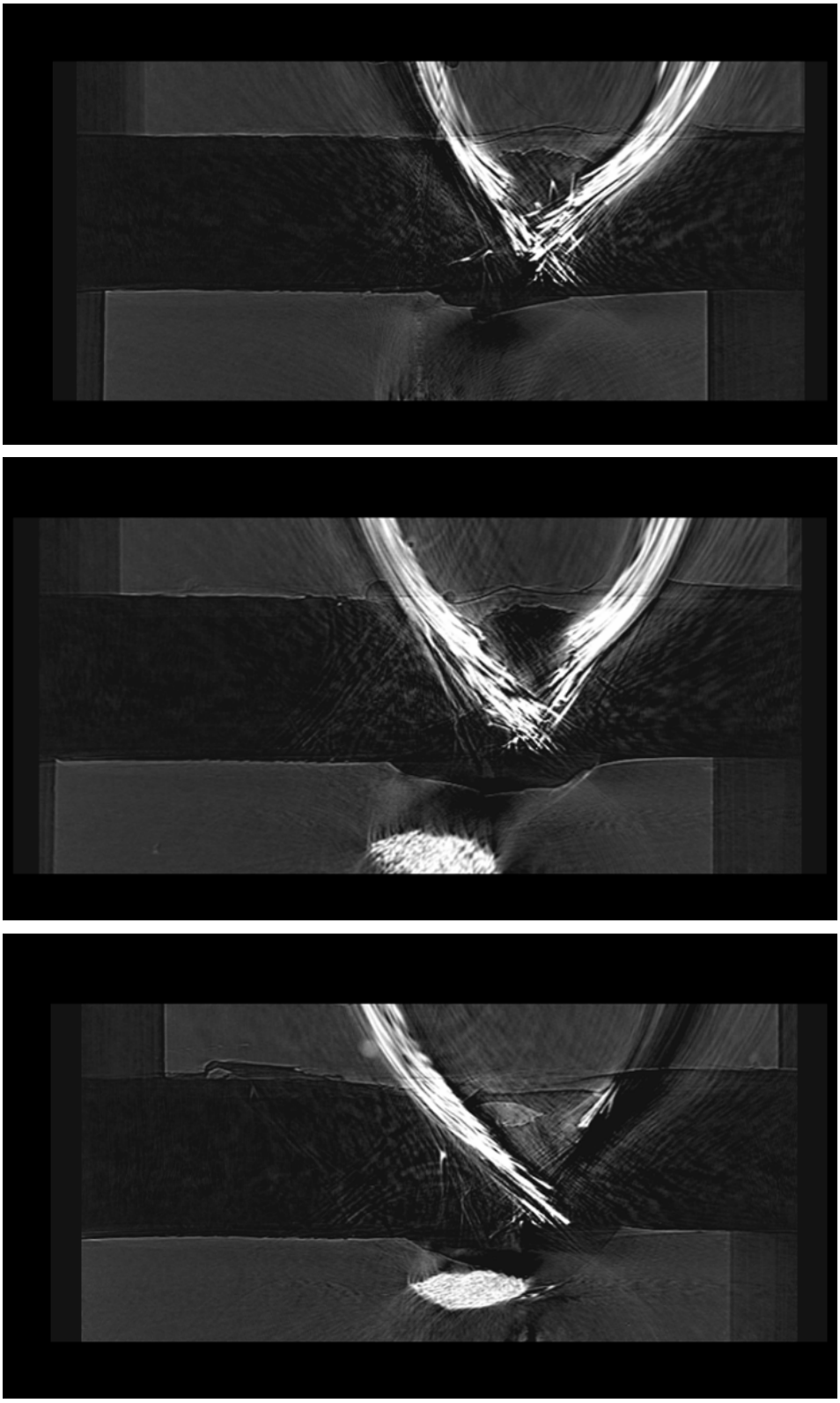

Figure 28. Selection of slices from a sequence of reconstruction slices showing failed specimen.

Conclusions

Test procedures and manufacturing techniques were developed for model composite specimens tested in a unique testing machine developed by ORNL within an x-ray micro-tomography unit. Three fiber forms were examined with failure occurring within the gage length for one of the fiber forms. Deformations within the material were observed using x-ray imaging as well as tomography reconstructions. Changes in the fiber form as well as crack development was visualized. Brittle failure at the grips for fiber forms without mold release applied to the fiber tow did not yield useful information about damage processes within the model composite specimen. Samples with tow coated with mold release exhibited observable crack growth prior to failure as well as fiber bridging requiring subsequent loading after initial failure. Internal and exposed crack surfaces formed in various directions with respect to the fiber tow and loading direction. It is believed that the techniques developed and demonstrated in this work can be further developed and utilized to better understand damage mechanisms for a variety of materials and loading situations.

Acknowledgements

This research was performed at the Oak Ridge National Laboratory (ORNL) and sponsored by Plastics Division of the American Chemistry Council under the Work-for-Others Program, IAN #14B578801, with the U.S. Department of Energy under contract DE-AC05-00OR22725 with UT-Battelle, LLC. The authors would also like to acknowledge AGY for supplying the fibers used in these experiments.

References

1. Reinhart T.J. et.al. (1987). *Engineered Materials Handbook Volume 1- Composites.* Metals Park, Ohio: ASM International.
2. Flesher N.D. (2006). *Crash Energy Absorption of Braided Composite Tubes*. Ph.D. Thesis, Stanford University.
3. Alpha Star Inc. (2003). *Genoa User's Manual*. Long Beach, California.
4. Dally J.W., & Riley W.F. (1991). *Experimental Stress Analysis* (3rd ed.). Knoxville, Tennessee: College House Enterprises.
5. Gao J., & Weitsman Y.J. (1998). *The Tensile Mechanical Properties and Failure Behavior of Stitched T300 Mat/Urethane 420 IMR Composite*. (Contract Technical Report). Knoxville, Tennessee: University of Tennessee.
6. Glennie, A. M. G. Gulley, T. J. (1985). *Acoustic Emission Modulus Determination and Source Location in Unidirectional Fibre Reinforced Polymer Composites*. J.Acoustic Emission. 170-173.
7. Deng S., & Weitsman Y.J. (2000). *Mechanical Response of Stitched T300 Mat/Urethane 420 IMR Composite Laminates: Property/Orientation Dependence and Damage Evolution*. ORNL/TM-2000/103.
8. AGY. *Fiberglass Continuous Filament Yarn For the Weaving Industry*. (2007). [On-line] Available: http://www.agy.com/products/eglass/PDFs/TP227LD.pdf.
9. Xradia Inc (2005). *MicroXCT User's Manual Version 2.0 Issue 1.1*. Concord, California.

10. Interface. *Model SML Low Height Load Cell*. (2007). [On-line] Available: http://www.interfaceforce.com/_products/documents/SML_51.pdf.
11. National Instruments. *NI Lab View*. (2007). [On-line] Available: http://www.ni.com/labview/.
12. Vlastimil Kunc et. al. *Development of Coupled Mechanical Testing and Computed X-ray Tomography Unit*. publication expected in 2008.